Robust multivariable microgrid control synthesis and analysis

Naderi M, Khayat Y, Batmani Y, and Bevrani H

Published (to be published) in: 3rd Int. Conf. on Power and Energy System Eng. (CPESE 2016), Kitakyushu, Japan,

(Expected) publication date: 2016

Citation format for published version:

Naderi M, Khayat Y, Batmani Y, and Bevrani H (2016) Robust multivariable microgrid control synthesis and analysis. in 3rd Int. Conf. on Power and Energy System Eng. (CPESE 2016), Kitakyushu, Japan, Sept. 2016.

Available online at www.sciencedirect.com

ScienceDirect

Energy Procedia 100 (2016) 375 – 387

Energy Procedia

3rd International Conference on Power and Energy Systems Engineering, CPESE 2016, 8-12 September 2016, Kitakyushu, Japan

Robust Multivariable Microgrid Control Synthesis and Analysis

M. Naderi, Y. Khayat, Y. Batmani, H. Bevrani*

Smart/Micro Grids Research Center, Dept. of Electrical and Computer Eng., University of Kurdistan, PO Box 416, Sanandaj, Iran.

Abstract

In this paper, an islanded microgrid is modelled as a linear multivariable dynamic system. Then, the multivariable analysis tools are employed. The generalized Nyquist diagram and the relative gain array are used respectively for the stability assessment and solving the paring problem among the inputs and outputs. Droop control dependency on the X/R ratio of the microgrid DERs is recognized and its type is proposed using the relative gain array concept. Robust stability, nominal performance and robust performance requirements are evaluated in order to a better understanding of the system dynamics. Finally, three different controllers including H_∞, H_2 and sequential proportional-integral-derivative controls are designed and compared.

Peer-review under responsibility of the organizing committee of CPESE 2016

Keywords: Microgrid; RGA; Generalized Nyquist; Robust performance; H_∞ control; H_2 control, Multivariable system.

1. Introduction

With the advent of small-scale power plants in the vicinities of distribution systems, some issues like huge losses related to bulk fossil power plants and transmission lines [1–3], construction cost of large generation units, dramatically decreased [4]. On the other hand, a number of environmental benefits such as clean and green environmentally advantages of distributed energy resources (DERs), are the other promising solutions of small-scale power plants and distributed generations (DGs) [5]. These new micro power plants, known as microgrids, can be connected or islanded from the legacy grids. Their improved efficiency, reliability, utilization of clean and various renewable energy resources, and expandability have been gained popularity of these networks more and more [6]. However, different dynamic properties of such systems, impressed the power system dynamics totally, and has

E-mail address: bevrani@ieee.org

Peer-review under responsibility of the organizing committee of CPESE 2016
doi:10.1016/j.egypro.2016.10.191

raised some crucial considerations at the integration of DGs with various energy resources [7]. Distributed generations with DC-output, e.g., PV arrays, energy storage elements and fuel cells, are generally connected to the AC microgrid distribution network by grid interface converters [8] such as voltage-source converters (VSCs). All of these cause some challenges in control and stability of microgrids, especially during islanded operation mode due to low or no inertia, nonlinear and wrapped dynamics, intermittent wind power and photovoltaic outputs, etc. [9].

The above mentioned issues motivate researchers to figure out detailed models of microgrids and DGs. Currently, surveys of the microgrid modelling and stability are mostly focus on the mathematical analysis and modelling of the microgrid to improve stability. Detailed consideration is paid to the small signal and transient stability analysis [10–16].

However, due to the intermittent nature of DERs and their uncertainties, it has encouraged many of researchers to design controllers based on the robust control strategies as powerful methodologies to achieve robust stability and performance in the presence of uncertainties [17]. Robust control strategies guarantee robust stability and provide desired performance specifications such as excellent transient response and zero steady-state error despite any type of un-modelled uncertainties in the system dynamics and possible perturbations and distortions [18].

This paper presents multivariable robust control strategies based on H_∞ and H_2 theorems for two connected VSC-coupled DG units that simultaneously supply a resistive load in the islanded operation mode. The mathematical equations of the studied system develops a dynamic model of two DERs and their common load in *dq* rotating frame, and presents a systematic approach for system recognition from the controllability and observability point of view. Also, for the obtained dynamic model, the generalized Nyquist stability criterion, and input-output sets selection are outlined. Finally, in order to enumeration of robust stability and performance needs, a standard control framework for robust control synthesis considering both structured an unstructured uncertainties are represented.

The rest of this paper is organized as follows. Section 2 presents the microgrid modelling using Park transformation. In Section 3, microgrid analysis as a multivariable system is presented. The uncertainty determination is presented in Section 4. In section 5, robust stability and performance requirements are given, robust H_∞ and H_2 controllers are designed and some simulations are performed.

2. Microgrid modelling using Park transformation

The schematic block diagram of the considered microgrid is depicted in Fig. 1 (a). In order to find a linear model of the microgrid, each DER is considered as a VSC with a static dc link, and the VSC is modeled by a controllable three-phase sinusoidal voltage source. The VSC output filter, transformer and line between the VSC and point of common coupling (PCC) are modeled by an equivalent inductance and an equivalent resistance. The load is considered as a common resistive in the PCC. Fig. 1 (b) shows the equivalent single-line diagram of the microgrid.

In order to find a linear time invariant (LTI) model of the microgrid, the most commonly method is converting the three-phase circuit equations to the *dq0* frame using Park transformation [19–22]. Park transformation converts three-phase voltages and currents to their *dq0* components, respectively. This transformation can be represented as follows:

$$\begin{bmatrix} f_d \\ f_q \\ f_0 \end{bmatrix} = \frac{2}{3} \begin{bmatrix} \cos(\theta) & \cos\left(\theta - \frac{2\pi}{3}\right) & \cos\left(\theta + \frac{2\pi}{3}\right) \\ -\sin(\theta) & -\sin\left(\theta - \frac{2\pi}{3}\right) & -\sin\left(\theta + \frac{2\pi}{3}\right) \\ \frac{1}{2} & \frac{1}{2} & \frac{1}{2} \end{bmatrix} \begin{bmatrix} f_a \\ f_b \\ f_c \end{bmatrix}, \tag{1}$$

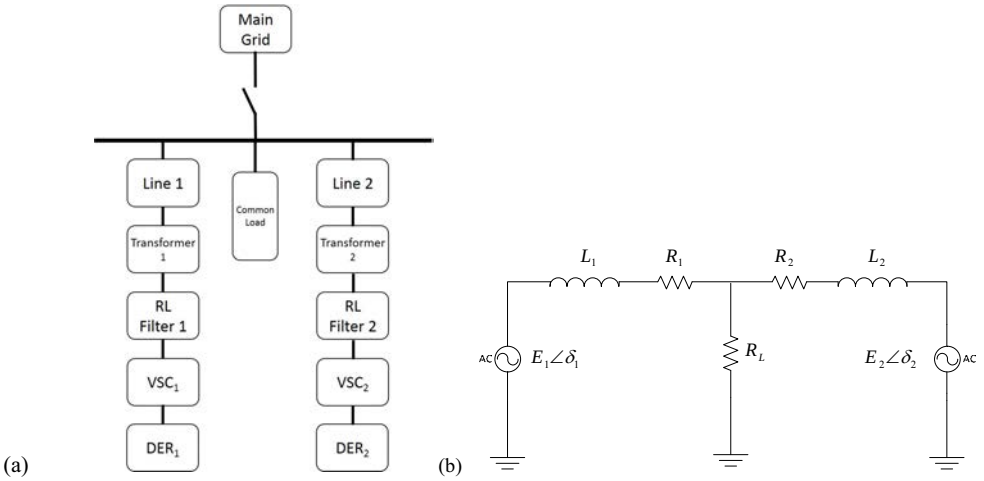

Fig. 1. Microgrid case study; (a) configuration, and (b) Single-line diagram.

where, f_d, f_q, f_0 are the direct, quadratic and zero components, respectively. The θ is rotation angle, and f_a, f_b, f_c are the balanced three-phase components. Under a balanced condition, the zero-sequence of the three-phase variable $\bar{f}_{abc} = [f_a \quad f_b \quad f_c]^T$ in (1) is zero ($f_0 = 0$). In this case, the Park transformation can be composed by the following two transformations:

$$\bar{f}_{\alpha\beta} = \frac{2}{3}(e^{j0} \quad e^{j\frac{2\pi}{3}} \quad e^{-j\frac{2\pi}{3}})\bar{f}_{abc}, \tag{2}$$

$$\bar{f}_{dq} = \bar{f}_{\alpha\beta} e^{-j\theta}, \tag{3}$$

where, $\bar{f}_{abc}$ is a 3×1 vector representing a balanced three-phase variable, $\bar{f}_{\alpha\beta} = f_\alpha + jf_\beta$ and $\bar{f}_{dq} = f_d + jf_q$. In (3), the $\theta = \omega_0 t + \theta_0$ is the phase-angle of the system three-phase voltages which is usually obtained using a phase-locked loop (PLL).

Using the KVL and the KCL and considering Fig.1 (b), the dynamical equations of the microgrid in *abc*-frame can be obtained, and after some manipulations, the following differential equations are achieved:

$$\begin{aligned}
\frac{di_{d1}}{dt} &= -(\frac{R_1+R_L}{L_1})i_{d1} + \omega_0 i_{q1} - \frac{R_L}{L_1}i_{d2} + \frac{1}{L_1}e_{d1},\\
\frac{di_{q1}}{dt} &= -\omega_0 i_{d1} - (\frac{R_1+R_L}{L_1})i_{q1} - \frac{R_L}{L_1}i_{q2} + \frac{1}{L_1}e_{q1},\\
\frac{di_{d2}}{dt} &= -\frac{R_L}{L_2}i_{d1} - (\frac{R_2+R_L}{L_2})i_{d2} + \omega_0 i_{q2} + \frac{1}{L_2}e_{d2},\\
\frac{di_{q2}}{dt} &= -\frac{R_L}{L_2}i_{q1} - \omega_0 i_{d2} - (\frac{R_2+R_L}{L_2})i_{q2} + \frac{1}{L_2}e_{q2}.
\end{aligned} \tag{4}$$

Using (1), the direct and quadratic components of the VSC output voltage are obtained as follows

$$e_d = E\sin(\delta),\ e_q = -E\cos(\delta) \tag{5}$$

where, E and δ are the VSC voltage amplitude and phase angle, respectively. Since these voltages are dependent to

each other, their components (E and δ) could be selected as control inputs. Hence, the standard state space model of the microgrid as a multivariable system is obtained by substituting (5) in (4). Linearized form of the resulted equations around the equilibrium points are

$$\frac{d}{dt}\begin{bmatrix}\Delta i_{d1}(t)\\ \Delta i_{q1}(t)\\ \Delta i_{d2}(t)\\ \Delta i_{q2}(t)\end{bmatrix}=A\begin{bmatrix}\Delta i_{d1}(t)\\ \Delta i_{q1}(t)\\ \Delta i_{d2}(t)\\ \Delta i_{q2}(t)\end{bmatrix}+B\begin{bmatrix}\Delta\delta_1(t)\\ \Delta E_1(t)\\ \Delta\delta_2(t)\\ \Delta E_2(t)\end{bmatrix},$$
$$\begin{bmatrix}\Delta i_{d1}(t)\\ \Delta i_{q1}(t)\\ \Delta i_{d2}(t)\\ \Delta i_{q2}(t)\end{bmatrix}=I_4\begin{bmatrix}\Delta i_{d1}(t)\\ \Delta i_{q1}(t)\\ \Delta i_{d2}(t)\\ \Delta i_{q2}(t)\end{bmatrix}+0_4\begin{bmatrix}\Delta\delta_1(t)\\ \Delta E_1(t)\\ \Delta\delta_2(t)\\ \Delta E_2(t)\end{bmatrix}, \tag{6}$$

where

$$A=\begin{bmatrix}\frac{-(R_1+R_L)}{L_1} & \omega_0 & \frac{-R_L}{L_1} & 0\\ -\omega_0 & \frac{-R_1}{L_1} & 0 & 0\\ \frac{-R_L}{L_2} & 0 & \frac{-(R_2+R_L)}{L_2} & \omega_0\\ 0 & 0 & -\omega_0 & \frac{-R_2}{L_2}\end{bmatrix},B=\begin{bmatrix}\frac{E_{10}\cos\delta_{10}}{L_1} & \frac{\sin\delta_{10}}{L_1} & 0 & 0\\ \frac{E_{10}\sin\delta_{10}}{L_1} & -\frac{\cos\delta_{10}}{L_1} & 0 & 0\\ 0 & 0 & \frac{E_{20}\cos\delta_{20}}{L_2} & \frac{\sin\delta_{20}}{L_2}\\ 0 & 0 & \frac{E_{20}\sin\delta_{20}}{L_2} & -\frac{\cos\delta_{20}}{L_2}\end{bmatrix} \tag{7}$$

In the above equations, δ_{10} and δ_{20} are the steady state values of $\delta_1(t)$ and $\delta_2(t)$, respectively.

3. Microgrid analysis as a multivariable system

The considered microgrid system has four inputs, four outputs and four state variables. Therefore, the transfer function matrix is a 4×4 frequency variable matrix where each entity is a fourth order transfer function. For the microgrid parameters presented in Table 1, the state and input matrices (7) and the related transfer function matrix are obtained as follows:

$$A=\begin{bmatrix}-128.4 & 314.16 & -0.093 & 0\\ -314.16 & -128.3 & 0 & 0\\ -0.125 & 0 & -107.05 & 314.16\\ 0 & 0 & -314.16 & -106.92\end{bmatrix},B=\begin{bmatrix}0.0853 & 0.0081 & 0 & 0\\ 0.0086 & -0.0812 & 0 & 0\\ 0 & 0 & 0.1118 & 0.0088\\ 0 & 0 & 0.0089 & -0.1094\end{bmatrix}$$
$$G(s)=\left[g_{ij}(s)\right],\quad i,j=1,2,3,4$$

where each array $g_{ij}(s)$ is a 4th-order transfer function.

Using the obtained state space representation of the MG, one can see that the system is asymptotically stable. Since there are no input, output, and input-output decoupling zeros, the utilized state space representation is both controllable and observable. Nevertheless, there are four zero elements in the right open half plane which cause some difficulties in the sequential controller design procedure.

Since the MG is a multi-input multi-output (MIMO) system, for designing of decentralized controllers, the first step is to choose proper pair of input and output. Indeed, it should be determined for any output which control input must be used. The *dq* currents exporting is one of the most common output set selections [21], which leads to a

strictly proper transfer function matrix. Another choice is $\{V_{d,PCC}, V_{q,PCC}\}$ in the islanded mode where the microgrid needs to control the voltage and frequency, locally [23]. In addition to input and output sets selection, the coupling between them is a key point in the controller design. The relative gain array (RGA) is a useful index for inputs and outputs coupling which can be used to solve the pairing problem.

Definition 1 The RGA of a non-singular square complex matrix G is a square complex matrix defined as

$$RGA(G) = \Lambda(G) = G \times (G^{-1})^T \tag{8}$$

where × denotes element-by-element multiplication [24]. The most desirable input-output couple has a positive RGA's element close to one. The obtained results, represented in Table 2, show that the solution of the pairing problem is depend on the X/R ratio. Indeed, it can be seen that in the first scenario, $\{\delta, i_q\}$ and $\{E, i_d\}$ are the best couples according to the RGA rule. However, for the last scenario, the RGA proposes to use of couples of $\{\delta, i_d\}$ and $\{E, i_q\}$ for decentralized control design procedure.

Table 1. Microgrid Parameters and linearization data

Parameters	Values	Parameters	Values
VSCs nominal power	7 MW	E_{10}	1.05 pu
VSCs nominal Voltage	4140 V	E_{20}	1.02 pu
Nominal frequency	50 Hz	δ_{10}	0.1 pu
L_1	95.5 mH	δ_{20}	0.08
L_2	71 mH	X_1/R_1	1
R_L	2.78 Ω	X_2/R_2	1.2

Table 2. Three microgrid output X/R with the corresponding RGAs

Scenario	1	2	3
$(X/R)_1,(X/R)_2$	0.3 , 0.4	1 , 1.2	4 , 5
RGA	$\begin{pmatrix} 0.39 & 0.61 & 0 & 0 \\ 0.61 & 0.39 & 0 & 0 \\ 0 & 0 & 0.28 & 0.72 \\ 0 & 0 & 0.72 & 0.28 \end{pmatrix}$	$\begin{pmatrix} 0.78 & 0.22 & 0 & 0 \\ 0.22 & 0.78 & 0 & 0 \\ 0 & 0 & 0.84 & 0.16 \\ 0 & 0 & 0.16 & 0.84 \end{pmatrix}$	$\begin{pmatrix} 0.96 & 0.04 & 0 & 0 \\ 0.04 & 0.96 & 0 & 0 \\ 0 & 0 & 0.97 & 0.03 \\ 0 & 0 & 0.03 & 0.97 \end{pmatrix}$

4. Uncertainty determination

The first step in the robust stability and performance analysis and control synthesis is the uncertainty formulation. In order to assess the robust stability and performance requirements, the parametric uncertainties is significant [25]. In addition, we want to design H_∞ and H_2 controllers for the microgrid; therefore, an unstructured uncertainty model is also needed. In this paper, $\pm 30\%$ changes in the load resistance is considered as the uncertainty.

4.1. Unstructured uncertainty modelling

The unstructured uncertainty is modelled in the following four steps:

1) Parametric uncertainty determination by considering 30% variation in the load resistance as follows:
$$R_L = R_{Ln}(1 + r\delta_r), \tag{9}$$
where R_{Ln} is the nominal resistance load, $|\delta_r| \le 1$ and $r = 0.3$.
2) Converting the parametric uncertainty to the unstructured uncertainty by considering an input multiplicative uncertainty model using the following formulation:

$$\hat{G}(s) = G_n(s)(1+\Delta_u(s)),$$
$$\Delta_u(s) = G_n(s)^{-1}(\hat{G}(s) - G_n(s)), \quad (10)$$

where $\hat{G}(s)$ and $G_n(s)$ are the transfer function matrices of the uncertain and nominal systems, respectively; and $\Delta_u(s)$ is the uncertainty transfer function matrix block.

3) Cure fitting for any element of the $\Delta_u(s)$ by a first or second order transfer function
4) Generating the weighting function such that

$$\Delta_u(s) = W_u(s).\Delta(s) \quad ; \left\|\Delta(s)\right\|_\infty \le 1 \quad (11)$$

$W_u(s)$ is a 4×4 weighting transfer function matrix which all entities are the first order transfer functions (high/low pass filters) as follows:

$$W_u(s) = \begin{pmatrix} \frac{46s+39450}{s+852} & \frac{113s+1.2\times10^5}{s+2295} & \frac{43s+27690}{s+620} & \frac{77s+57280}{s+1148} \\ \frac{109s+10^5}{s+2102} & \frac{46s+28770}{s+612} & \frac{78s+60290}{s+1175} & \frac{43s+32210}{s+726} \\ \frac{46s+22090}{s+465} & \frac{80s+49480}{s+1035} & \frac{43s+18380}{s+413} & \frac{110s+11040}{s+2270} \\ \frac{78s+49090}{s+1017} & \frac{46s+3992}{s+85} & \frac{109s+10^5}{s+2049} & \frac{43s+19050}{s+429} \end{pmatrix} \quad (12)$$

4.2. Parametric uncertainty modelling

Fig. 2 shows the block diagram of the system, which shows only connections between the control inputs and the state variables. As mentioned already, the only uncertain parameter is the load resistance. The load resistance block's inputs are Δi_{d1} and Δi_{d2}, and its outputs are Y_1 and Y_2. Fig. 3 shows the procedure of the parametric uncertainty modelling, where $\Delta_r = \delta_r I_2$ and the matrix M_{R_L} is obtained as

$$M_{R_L} = \begin{bmatrix} R_{Ln} & 0 & rR_{Ln} & 0 \\ 0 & R_{Ln} & 0 & rR_{Ln} \\ 1 & 0 & 0 & 0 \\ 0 & 1 & 0 & 0 \end{bmatrix}. \quad (13)$$

The open loop transfer function matrix *M* is realized with the following state space equations

$$\dot{x}(t) = Ax(t) + B_u u(t) + B_w w(t)$$
$$y(t) = x(t) = Cx(t) + D_u u(t) + D_w w(t) \quad (14)$$
$$z_r(t) = C_r x(t)$$

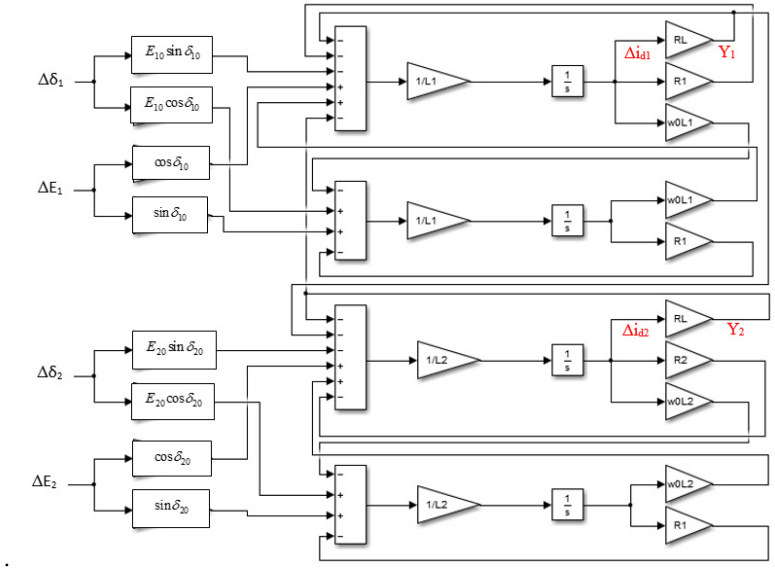

Fig. 2. System block diagram

where

$$B_u = B\ ,\quad C = \bar{I}_{4\times4}\ ,\quad D_u = \bar{0}_{4\times4}\ ,\quad D_{ur} = \bar{0}_{2\times4}\ ,\quad D_{wr} = \bar{0}_{2\times2}\ ,$$

$$B_w = \begin{bmatrix} -\frac{rR_{Ln}}{L_1} & 0 & -\frac{rR_{Ln}}{L_2} & 0 \\ -\frac{rR_{Ln}}{L_1} & 0 & -\frac{rR_{Ln}}{L_2} & 0 \end{bmatrix}^T,\quad C_r = \begin{bmatrix} 1 & 0 & 0 & 0 \\ 0 & 0 & 1 & 0 \end{bmatrix},$$

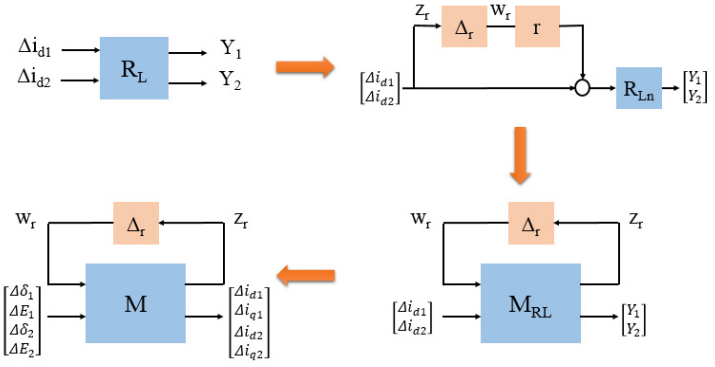

Fig. 3. Parametric uncertainty block modelling

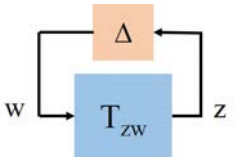

Figure 4. Closed-loop system for robust control analysis and synthesis

5. Robust stability and performance

In this section, robust stability, nominal and robust performance requirements are represented in the case of given two-DER microgrid. In addition, two robust controllers. i.e. H_∞ and H_2, and a sequential PID controller are designed and compared using the linearized model of the MG presented in Section 2.

5.1. Robust Stability Requirement

In order to use the standard H_∞ and H_2 control design procedures, the closed-loop structure, depicted in Fig. 4, is considered. Using the small gain theorem [18], the system without any controller is robustly stable if and only if $\|T_{wz}(s)\|_\infty \le \gamma$ and $\|\Delta(s)\|_\infty \le 1/\gamma$, where $T_{wz}(s)$ for different dynamic and uncertainty test scenarios. Table 3 shows the γ and the maximum acceptable uncertainty disc radius for three scenarios. For instance, the maximum infinity norm of $T_{wz}(s)$ for scenario 2 is 0.12. Hence, the maximum acceptable uncertainty disc radius to have a stable system is 8.33, i.e. $\|\Delta\|_\infty$ must be less than 8.33. However, this uncertainty limitation is too conservative due to its unstructured model. Results of robust stability requirements are compared in Table 3 for three scenarios.

5.2. Nominal and Robust Performance Requirement

For the problem at hand, having a desirable tracking, less control signal energy, and disturbance attenuation are considered as the performance objectives. Good tracking and disturbance attenuation are behaving in the same direction, but they should be compromised with the goal of less control signal energy. The next step in the performance assessment is weighting functions determination. There is not any exact and straightforward law for finding weighting functions. One may start by an initial weight and continue the tuning process concerning the closed-loop performance in a simulation environment. Some guidelines for tuning of weighting functions are given in [25].

The closed-loop system with selected weighting functions are shown in Fig. 5. The W_1, W_2, and W_3 are the weighting functions for obtaining desirable tracking, less control signal energy, and disturbance attenuation, respectively.

$$w_1(s) = \frac{1000(s+500)}{s+150} \quad \rightarrow \quad W_1(s) = \mathrm{diag}(w_1, w_1, w_1, w_1),$$

$$w_2(s) = \frac{s+2}{s+10} \quad \rightarrow \quad W_2(s) = \mathrm{diag}(w_2, w_2, w_2, w_2),$$

$$w_3(s) = \frac{0.01(s+5)}{s+0.045} \quad \rightarrow \quad W_3(s) = \mathrm{diag}(w_3, w_3, w_3, w_3).$$

In nominal open-loop performance analysis, the uncertainty and less control signal energy goals are not considered. Ignoring the second item is due to the absence of the controller. On the other hand, for the robust open-loop performance objectives, the uncertainty is considered while the second item is ignored due to the absence of the controller. Then, the open loop interconnection is found and the closed-loop transfer function matrices for nominal performance $G_{cl\text{-}np}(s)$ and robust performance $G_{cl\text{-}rp}(s)$ are obtained as follows:

$$\begin{bmatrix} z_1 \\ z_2 \end{bmatrix} = G_{cl-np} \begin{bmatrix} r \\ d \end{bmatrix}, \quad \begin{bmatrix} z \\ z_1 \\ z_2 \end{bmatrix} = G_{cl-rp} \begin{bmatrix} w \\ r \\ d \end{bmatrix} \tag{15}$$

Table 3. γ and maximum acceptable uncertainty disc radius for scenarios 1, 2 and 3

Scenario	1	2	3
$(X/R)_1,(X/R)_2$	0.3 , 0.4	1 , 1.2	4 , 5
γ	0.042	0.12	0.49
Uncertainty Radius	23.81	8.33	2.05

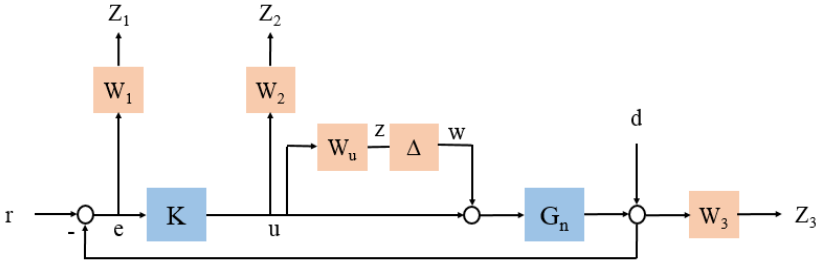

Figure 5. Closed-loop system diagram

5.3. Robust H_∞ Controller

The closed-loop structure shown in Fig. 5 is used for designing of robust H_∞ controller. Here, the weighting functions are chosen as follows:

$$w_1(s) = \frac{2\times10^5(s+120)}{s+15} \rightarrow W_1(s) = \mathrm{diag}(w_1, w_1, w_1),$$

$$w_2(s) = \frac{s+2}{s+10} \rightarrow W_2(s) = \mathrm{diag}(w_2, w_2, w_2),$$

$$w_3(s) = \frac{0.01(s+5)}{s+0.045} \rightarrow W_3(s) = \mathrm{diag}(w_3, w_3, w_3).$$

In order to design an H_∞ controller satisfying robust stability and robust performance requirements, the open loop interconnection of the transfer function matrices *G*, W_1, W_2, W_3 and *Wu* is found according to Fig. 5 and then the controller is designed using robust control tools in MATLAB software. Since the resulting robust controller usually has a big order, order reduction methods like residualization and truncation should be applied to reduce the order of the robust controller. Fig. 6 shows the frequency responses of the original controller and its reduced order using residualization and truncation methods. The original controller is obtained with order of 216 and reduced order controllers are 6th order. Generally, the residualization method in low frequencies and truncation method in high frequencies have a response similar to the original system. Fig. 7 shows the time responses of the original and reduced-order controllers. The time of the events is given in Table 4. According to Fig. 7, the residualization method has faster responses, but the steady state error of the truncation method is less. In addition, the system tracks the reference input well using the original and residualized controllers and the disturbance effects are less than 10 % (0.02 pu) in all times. The interaction between i_d and i_q of VSCs is mutually obvious in the step responses. In fact, when i_d is set on the desired value, i_q has had a certain amount and when output i_d and i_q of a VSC are set, other VSC has had a certain output. This behaviour is due to the operation of microgrid in islanding mode.

Table 4. Time of the events

Time (s)	0.1	0.2	0.3	0.4	0.6	0.7	0.8	0.9
Event	1 pu Step in i_{d1}	1 pu Step in i_{q1}	1 pu Step in i_{d2}	1 pu Step in i_{q2}	0.2 pu step in dist. 1	0.2 pu step in dist. 2	0.2 pu step in dist. 3	0.2 pu step in dist. 4

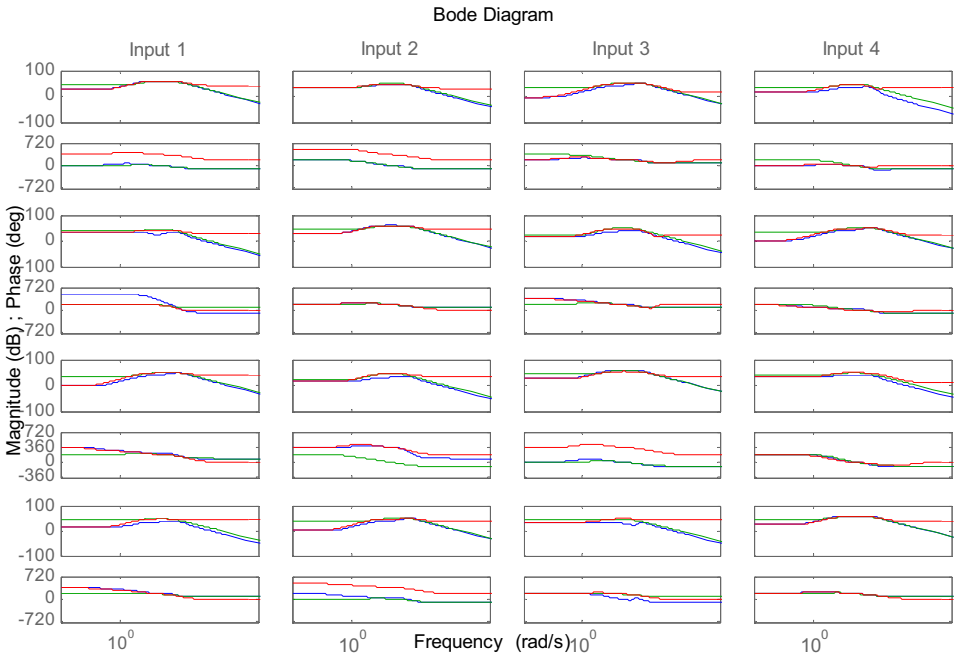

Figure 6. Frequency responses of the original H_∞ controller (red) and reduced-order controllers using residualization (blue) and truncation (green) methods

5.4. Robust H_2 Controller

All sections of the H_2 controller design is similar to the H_∞ controller design except the weighting functions. In H_2 controller design, strictly proper weighting transfer functions should be applied to have a strictly proper closed-loop transfer function, because the H_2 design method tries to minimize H_2 norm of the desired closed-loop transfer function whereas H_2 norm of the proper transfer functions is infinity. Therefore, weighting functions are obtained by trying and running again and paying attention to the recent point as follows:

$$w_1(s)=\frac{1.8\times10^6}{s+35} \quad \rightarrow \quad W_1(s)=\mathrm{diag}(w_1,w_1,w_1,w_1),$$

$$w_2(s)=\frac{100}{s+30} \quad \rightarrow \quad W_2(s)=\mathrm{diag}(w_2,w_2,w_2,w_2),$$

$$w_3(s)=\frac{0.05}{s+0.045} \quad \rightarrow \quad W_3(s)=\mathrm{diag}(w_3,w_3,w_3,w_3).$$

The time of the events is given in Table 4. Fig. 8 shows step responses of the closed-loop system for the original and reduced-order controllers. The original controller is obtained with order of 368 and reduced order controllers are 6th order. As can be seen, the truncation method cannot success in this scenario. It has an overshoot between 50%

and 100% for different outputs and its settling time is larger than 1s. However, the residualization method has very faster responses with the minimum possible steady state error. The controller order can be reduced to two.

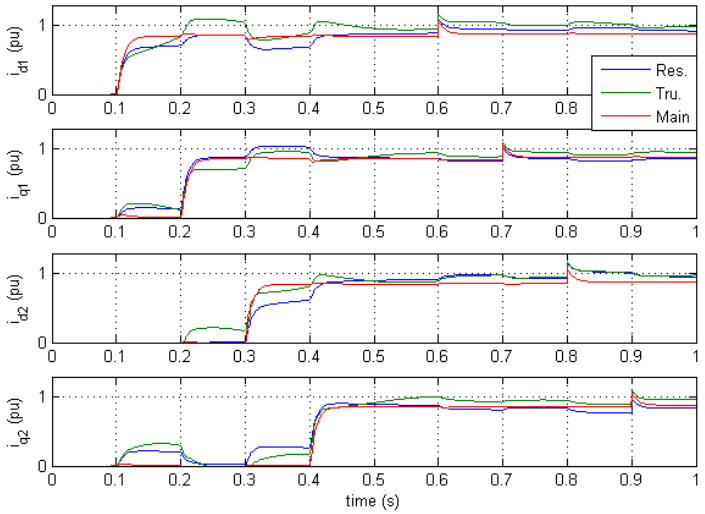

Figure 7. Time responses of the main H_∞ controller (red) and reduced-order controllers using residualization (blue) and truncation (green) methods

The truncated controller cannot track the reference inputs in considerable number of the cases whereas the residualized controller has a good performance yet. With comparison between Figs 6, 7 and 8, the enhanced performance using H_∞ and H_2 controller is obvious. Besides, Fig. 9 provides the comparison between sequential tuned PID, robust truncated H_∞ and residualized H_2 controllers. PID controller has a very large settling time despite it is tuned. This slow PID response may cause instability after a fault in the microgrid or main grid. The better performance of the robust truncated H_∞ and residualized H_2 controllers against tuned PID controller is visible considerably. However, the robust truncated H_∞ and residualized H_2 controllers have not impressive difference with each other. In both cases, the steady state error and maximum overshoot and undershoot are less than 0.7%, 20% and 25%, respectively.

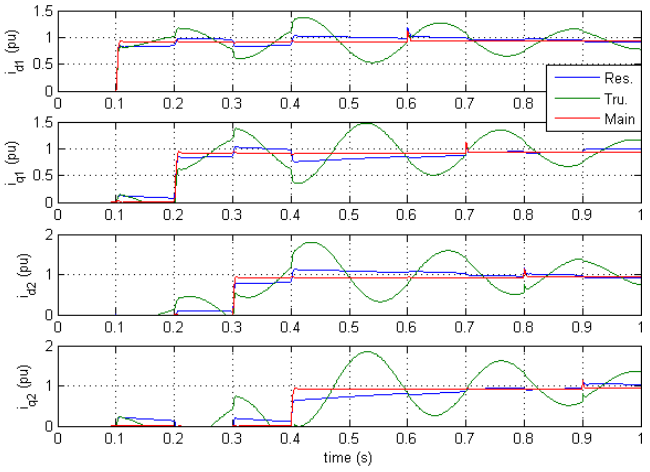

Figure 8. Time responses of the main H_2 controller (red) and 6th reduced-order controllers using residualization (blue) and

truncation (green) methods.

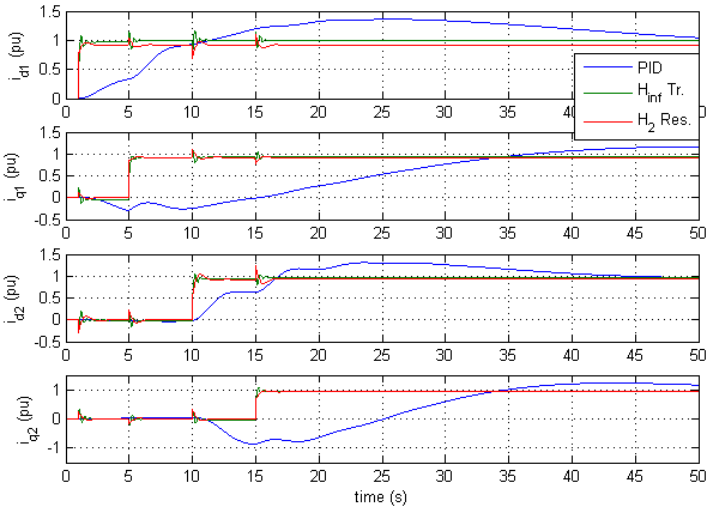

Figure 9. Time responses of the sequential tuned PID, robust truncated H_∞ and residualized H_2 controllers.

6. Conclusion

An LTI model has been obtained for the two-VSC islanded microgrid using Park transformation. The RGA has proposed couples $\{\delta, i_q\}$ and $\{E, i_d\}$ as an appropriate input-output couples for a very weak microgrid with DER's X/R ratios 0.3 and 0.4 and couples $\{\delta, i_d\}$ and $\{E, i_q\}$ for a rather weak microgrid with DER's X/R ratios 1 and 1.2 and a strong microgrid with DER's X/R ratios 4 and 5. The nominal and robust performance requirements have obtained. Two robust H_∞ and H_2 controllers have been designed, and the order of obtained controllers have been reduced from 368 and 216 to 6 and 2, respectively. The performances of the reduced-order controllers have been assessed and confirmed in MATLAB environment. It has been observed that the reduced order H_∞ controller (using the truncation method) and the reduced order H_2 controller (using the residualization method) have much better performance than the PID controller.

References

[1] Liserre, M., Sauter, T., & Hung John, Y. (2010). Future energy systems integrating renewable energy sources into the smart power grid through industrial electronics. *IEEE Industrial Electronics Magazine*, *4*(1), 18–37.

[2] Gertmar, L., Liljestrand, L., & Lendenmann, H. (2007). Wind energy powers-that-be successor generation in globalization. *IEEE Transactions on Energy Conversion*, *22*(1), 13–28.

[3] Huang, A. Q., Crow, M. L., Heydt, G. T., Zheng, J. P., & Dale, S. J. (2011). The future renewable electric energy delivery and management (FREEDM) system: the energy internet. *Proceedings of the IEEE*, *99*(1), 133–148.

[4] Jarrah, M. (2016). Modeling and simulation of renewable energy sources in smart grid using DEVS formalism. *Procedia Computer Science*, *83*, 642–647.

[5] Saheb-Koussa, D., Koussa, M., Belhamel, M., and Haddadi, M. (2011). Economic and environmental analysis for grid-connected hybrid photovoltaic-wind power system in the arid region. *Energy Procedia*, *6*, 361–370.

[6] Amer, M., Namaane, A., & M'Sirdi, N. K. (2013). Optimization of hybrid renewable energy systems (HRES) using PSO for cost reduction. *Energy Procedia*, *42*, 318–327.

[7] H. Bevrani, M. Watanabe, and Y. Mitani. Power system monitoring and control. Hoboken, NJ, USA: Wiley, Jun. 2014.

[8] Rocabert, J., Luna, A., Blaabjerg, F., and Rodriguez, P. (2012). Control of power converters in AC microgrids. *IEEE Transactions on Power Electronics*, *27*(11), 4734–4749.

[9] H. Bevrani, M. Watanabe, and Y. Mitani. Microgrid controls. *Standard handbook for electrical engineers.* New York, NY, USA: McGraw-Hill, 2012

[10] Pogaku, N., Prodanovic, M., & Green, T. C. (2007). Modeling, analysis and testing of autonomous operation of an inverter-based microgrid. *IEEE Transactions on power electronics*, *22*(2), 613–625.
[11] Bottrell N, Prodanovic M, Green TC. (2013) Dynamic stability of a microgrid with an active load. *IEEE Trans Power Electron*; 28: 5107–19.
[12] Lee, D. J., & Wang, L. (2008). Small-signal stability analysis of an autonomous hybrid renewable energy power generation/energy storage system part I: time-domain simulations. *IEEE Transactions on Energy Conversion*, *23*(1), 311–320.
[13] Vadana, D. P., & Kottayil, S. K. (2015). Autonomous control of smart microgrid in islanding mode. *Procedia Technology*, *21*, 204–211.
[14] Acevedo, S. S., & Molinas, M. (2012). Identifying unstable region of operation in a micro-grid system. *Energy Procedia*, *20*, 237–246.
[15] Jamroen, C., Namproom, P., & Dechanupaprittha, S. (2016). "TS-fuzzy based adaptive PEVs charging control for smart grid frequency stabilization under islanding condition," *Procedia Computer Science*, *86*, 124–127.
[16] Bevrani, H., Feizi, M. R., and Ataee, S. (2016). Robust frequency control in an islanded microgrid: H_{inf} and μ synthesis approaches. *IEEE Transactions on Smart Grid*, *7*(2), 706–717.
[17] H. Bevrani, "Robust power system frequency control," 2nd ed. Gewerbestrasse, Switzerland: Springer, 2014
[18] Zhou, K., & Doyle, J. C. (1998). *Essentials of robust control* (Vol. 104). Upper Saddle River, NJ: Prentice hall.
[19]Ashabani, Mahdi, and Yasser Abdel-Rady Mohamed. (2014). Integrating VSCs to weak grids by nonlinear power damping controller with self-synchronization capability. *IEEE Transactions on Power Systems* 29.2: 805–814.
[20] Mishra, Shivakant, D. Ramasubramanian, and P. C. Sekhar. (2013). A seamless control methodology for a grid connected and isolated PV-diesel microgrid. *IEEE Transactions on Power Systems* 28.4 (2013): 4393–4404.
[21] Ashabani, Mahdi, and Yasser Abdel-Rady Mohamed. (2014). Multivariable droop control of synchronous current converters in weak grids/microgrids with decoupled *dq*-axes currents. *IEEE Transactions on Smart Grid*.
[22] Kundur, Prabha, Eds. Neal J. Balu, and Mark G. Lauby. (1994). *Power system stability and control*. Vol. 7. New York: McGraw-hill.
[23] Babazadeh, Maryam, and Hamid Reza Karimi. (2013). A robust two-degree-of-freedom control strategy for an islanded microgrid. *IEEE Transactions on Power Delivery* 28.3: 1339–1347.
[24] Albertos, P., and A. Sala. (2004). *Introduction to multivariable control systems: An Engineering Approach*: 82–90.
[25] Bevrani H. Robust Power System Frequency Control. 2nd Ed., Springer, Switzerland, 2014.